Manuscript submitted to: Volume 3, Issue 2, 184-200.

AIMS Energy DOI: 10.3934/energy.2015.2.184

Received date 29 December 2014, Accepted date 14 April 2015, Published date 24 April 2015

Research article

Analysis of Passive RF-DC Power Rectification and Harvesting Wireless RF Energy for Micro-watt Sensors

Antwi Nimo*, Tobias Beckedahl, Thomas Ostertag and Leonhard Reindl

University of Freiburg, Department of Microsystems Engineering - IMTEK. Laboratory for Electrical Instrumentation. Georges-Köhler-Allee 106, 79110 Freiburg, Germany

* **Correspondence:** Email: antwi.nimo@imtek.de or reindl@imtek.de; Tel: +49-761-203-7221; Fax: +49-761-203-7222.

Abstract: In this paper, analytical modeling of passive rectifying circuits and the harvesting of electromagnetic (EM) power from intentionally generated as well as from ubiquitous sources are presented. The presented model is based on the linearization of rectifying circuits. The model provides an accurate method of determining the output characteristics of rectifying circuits. The model was verified with Advance Design System (ADS) Harmonic balance (HB) simulations and measurements. The results from the presented model were in agreement with simulations and measurements. Consequently design considerations and trade-off of radio frequency (RF) harvesters are discussed. To verify the exploitation of ambient RF power sources for operation of sensors, a dual-band antenna with a size of ~λ/4 at 900 MHz and a passive dual-band rectifier that is able to power a commercial Thermo-Hygrometer requiring ~1.3 V and 0.5 MΩ from a global system for mobile communications (GSM) base station is demonstrated. The RF power delivered by the receiving dual-band antenna at a distance of about 110 m from the GSM base station ranges from −27 dBm to −50 dBm from the various GSM frequency bands. Additionally, wireless range measurements of the RF harvesters in the industrial, scientific and medical (ISM) band 868 MHz is presented at indoor conditions.

Keywords: Ambient RF energy harvesting; Schottky diode rectifier; dual-band RF harvester; rectenna; RF to DC rectification model; wireless power transmission

1. Introduction

Recent advances in lowering power demands of wireless remote sensors has afforded the ability to power these sensors with micro-watt power levels. In situations where periodic change of the

batteries is not desired, powering the sensors through wireless power sources provides an effective alternative. As a result, wireless RF energy harvesting from ambient sources or from dedicated transmitters has gained research interest for use in these sensor systems. The major challenge in passive wireless energy harvesting is the efficient transformation of the input EM power levels that are less than −10 dBm to the voltage and current demands of the direct current (DC) load. A passive RF to DC power harvester must be optimized at each stage of the circuit design for true implementation of this energy harvesting approach. An RF power harvester consists of a receiving antenna, an impedance matching/transformation network, DC power conditioning and or management and the wireless sensor to be powered. Figure 1 shows a schematic of a passive wireless RF energy harvester. The rectifier may be a single diode or diode-connected transistor, or a cascade of rectifiers. In-between the antenna and the rectifier is an impedance matching or transformation network. The matching network consists of passive components providing inductive or capacitive reactance. The load represents the DC storage or transformation elements and the sensor to be powered.

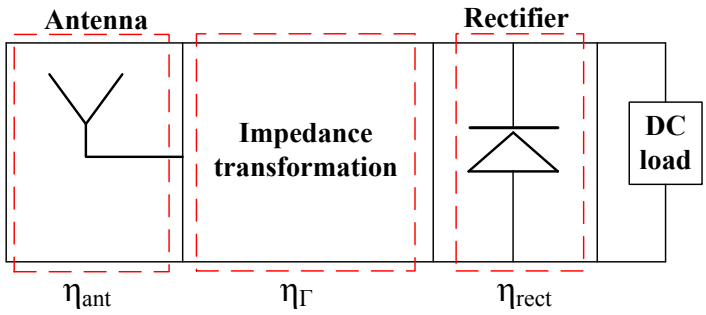

Figure 1. Block diagram of a passive wireless RF energy harvester. η_{ant}, η_{Γ} and η_{rect} are the efficiencies of the receiving antenna, impedance transformation network and the rectifier respectively.

The design of fully passive RF harvesters lies in the accurate modeling of the complete rectifier circuit so that its output performance can be predicted. Harrison et al. [1] used Ritz-Galerkin analysis to present the DC output characteristics of a single diode rectifier with some restrictions. The model neglects the diode junction capacitance and therefore the output DC voltage dependence on the operating frequency. A closed-form equation was presented in [2] that approximates a diode rectifier efficiency and input impedance. In [3,4], models that predict the conversion efficiency of an N-stage full-wave rectifier was presented. However, the DC load current must be determined or maintained to satisfy the constraints in the model. HB simulations using Agilent ADS software can be used to determine the output DC voltage of a rectifier circuit, however it is computationally intensive and do not easily provide the global view of the circuit response [1].

In this paper, a linearized model is presented to determine the output behavior of rectifying circuits. The model assumes steady state conditions and may be applied at various input power levels and connected DC load resistance without neglecting the impedance matching effects and the dynamic influence of the diode impedance on the rectifying process.

With the appropriate design of a rectifier circuit, ambient electromagnetic power harvesters may

be realized. In our previous work [5,6], wireless RF power transfer were presented in the ISM bands using intentionally generated sources. In [7,8] and [9], ambient RF power harvesters from television (TV) transmitting base stations at the frequency band of (450 to 770) MHz were presented. In [7] for example, the TV base station transmitting about 960 kW was able to power sensors requiring up to 60 μW at a distances of 4.1 km. In [8] and [9], it was shown that a single TV base station can provide multiple TV channels for harvesting. However published work using ambient TV base station signals relies on antenna sizes in the range of 1.5 A4 size or larger for harvesting. These antenna sizes corresponds to at least half of the operating wavelength at (450 to 770) MHz. A rectenna that is larger than A4 size hinder practical integration of the system into modern wireless sensors. In [10], a survey was made to prove the possibility of harvesting RF energy from ambient sources such as GSM. GSM base station transmitters may be the most available in urban environments due to the immense availability of cellular network providers.

In this paper, an ISM band 868 MHz and ambient GSM wireless RF harvester is presented. Planar antenna sizes as small as 6 cm × 8 cm (~λ/4 at 900 MHz) may be used with the rectifier for ubiquitous RF harvesting. The rectifier is designed to operate with dual-band frequency. Using this approach, ubiquitous RF power sources in the range of −27 dBm to −50 dBm and from different frequencies can be utilized for continuous operation of micro-watt sensors.

This paper is structured as follows. Section 2 presents the rectifying circuits and the linearized analytical model. Section 3 presents the verification of the model and its comparison to ADS software HB simulations and measured results. Section 4 presents the design consideration and trade-off when realizing RF power harvesters. The design considerations are based on the presented model. Section 5 presents harvesting RF power from intentionally generated sources at indoor conditions and from ubiquitous sources using a GSM base station at outdoor conditions. Conclusions are given in section 6.

2. Analysis of rectifying circuits

2.1. Efficiency versus voltage sensitivity

Efficiency η is defined as in (1), where P_L is the output DC power and P_A is the input RF power. The voltage sensitivity γ is given by (2), where V_L is the output DC voltage.

$$\eta = \eta_{ant} \times \eta_{\Gamma} \times \eta_{rect} = \frac{P_L}{P_A} \tag{1}$$

$$\gamma = \frac{V_L}{P_A} \tag{2}$$

The current state of the art of low power sensors would require a DC voltage supply of about 1 V and DC current of 10 μA. Therefore, it is necessary to specify the output voltage and current separately rather than the product, the DC output power, when considering RF energy harvesters for remote sensors [4,11]. The delivered input RF power P_A from the receiving antenna must be transformed to that minimum voltage required to energize the sensor. Although the efficiency is widely presented in literature, its practical use in ambient RF energy harvesting can be limited. This is because an RF harvester can deliver an output DC power more than what is required by a remote sensor but may be unable to energize the sensor due to its specific voltage and input current demands.

Therefore, voltage sensitivity of a passive RF harvester may be more important than the output efficiency when powering DC loads from micro-watt RF power levels, as such more emphasis is placed on the γ rather than η in this paper.

2.2. RF diode equivalent circuit model

As shown in Figure 1, an impedance transformation network is a sub-system of a wireless RF harvester. The impedance transformation network filters higher order impedances of the diode at the operating frequency. For this reason, only the diodes fundamental impedance at the frequency of operation may be required for its accurate modeling in RF energy harvesting applications. A packaged Schottky diode may be modeled as a nonlinear junction resistance R_j shunted by a non-linear junction capacitance C_j. V_j is the voltage loss at the rectifying junction. R_S, L_S and C_P are the bulk resistance, packaging inductance and capacitance respectively [12]. A bare diode may also be modeled as a voltage controlled junction current source in parallel with a controlled capacitance (see Figure 2) and a parasitic bulk resistance [13]. I_{DC} is the voltage controlled current source from the rectifying junction. Without neglecting the bulk resistance and the package parasitics, the controlled current source is treated as a DC source in parallel with a conductance G and a susceptance B. R_D and X_D are the parallel resistance and reactance of the diode respectively. I_{DC}, R_D and X_D as in the linearized model are variables which depend on the diode parameters, input RF power P_A, the connected DC load and the reflection coefficient at the input of the rectifier.

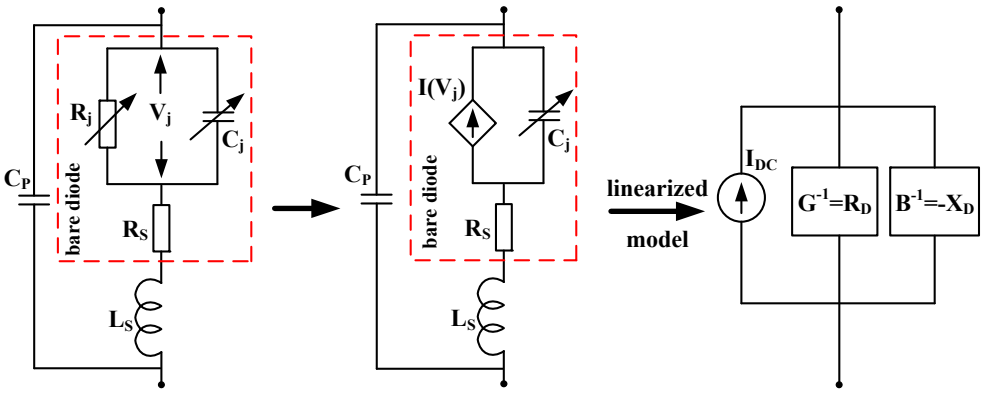

Figure 2. Schottky diode equivalent circuit models.

From Figure 2 (Left), the admittance of a Schottky diode may be written as in (3), where Y_{diode} is the diode admittance.

$$Y_{diode} = G + jB = \left(\frac{-jR_j \frac{1}{\omega C_j}}{R_j - \frac{j}{\omega C_j}} + R_S + j\omega L_S \right)^{-1} + j\omega C_P \tag{3}$$

Equation (3) can be expanded into the conductance G and susceptance B. The expression for C_j [13] is given by (4). Where Q is the charge stored at the rectifying junction.

$$C_j = \frac{\partial Q}{\partial V_j} \tag{4}$$

R_j can be found from Richardson's equation [14], which describes the current voltage relationship at the rectifying junction of a Schottky diode. The current voltage relationship at the rectifying junction is given by (5).

$$I = I_S\left[exp\left(\frac{qV_j}{\eta_0 KT}\right) - 1\right] \tag{5}$$

I_S is the diode reverse saturation current, $\alpha = \frac{KT}{q}$. α is the thermal voltage. η_0 is the diode ideality factor. q is the charge of an electron. T is the temperature and K is the Boltzmann constant. Since I is an infinite series with higher order values, there are higher order values of the diode junction resistance R_j.

$$R_j = \left(\frac{\partial I}{\partial V_j}\right)^{-1} = \frac{\eta_0 \alpha}{I_S + I} \tag{6}$$

I varies with changes in the input RF power level P_A, the losses in the impedance transformation network, rectifier impedance or connected DC load. It is easily deduced from (6) that the magnitude of I also affects the junction resistance R_j and consequently the overall impedance of the diode. Due to this, the input impedance of a diode must always be measured at a specified RF power level and DC load conditions.

The effect of a Schottky diode equivalent circuit parameters on the parallel resistance $(R_D = 1/G)$ is presented. This allow for direct comparison of each diode parasitic parameter on the R_D. The diode parasitic parameters which were used in calculating the diode impedance are shown in Table 1. V_{BV} is the reverse breakdown voltage of the Schottky diode.

Table 1. The Spice parameters of HSMS-286 Schottky diode.

I_S (nA)	I (nA)	C_j (pF)	R_S (Ω)	L_S (nH)	C_P (pF)	V_{BV} (V)
50	2	0.18	6	2	0.08	7

Figure 3(Top-left) shows the effect of the saturation current I_S on the diode rectifying junction voltage losses V_j, for various values of I. At I in the range of 5 μA, the V_j across both the I_S = 0.5 μA and the I_S = 50 nA approaches zero. When the I passing through the diode rectifying junction is greater than about 0.05 mA, the efficiency of rectification is skewed to the one with I_S = 0.5 μA, since the peak V_j of the diode with I_S = 50 nA is much higher at this condition. The results show that the smaller the I that goes through a Schottky diode rectifying junction, the smaller the V_j across it. Therefore the η_{rect} of a Schottky diode increases with high input voltage instead of high input current. Hence maximum voltage transformation at the input of the diode rectifier is always necessary for its efficient operation. The voltage transformation of the input RF power will reduce the amount of

current passing through the diode rectifying junction.

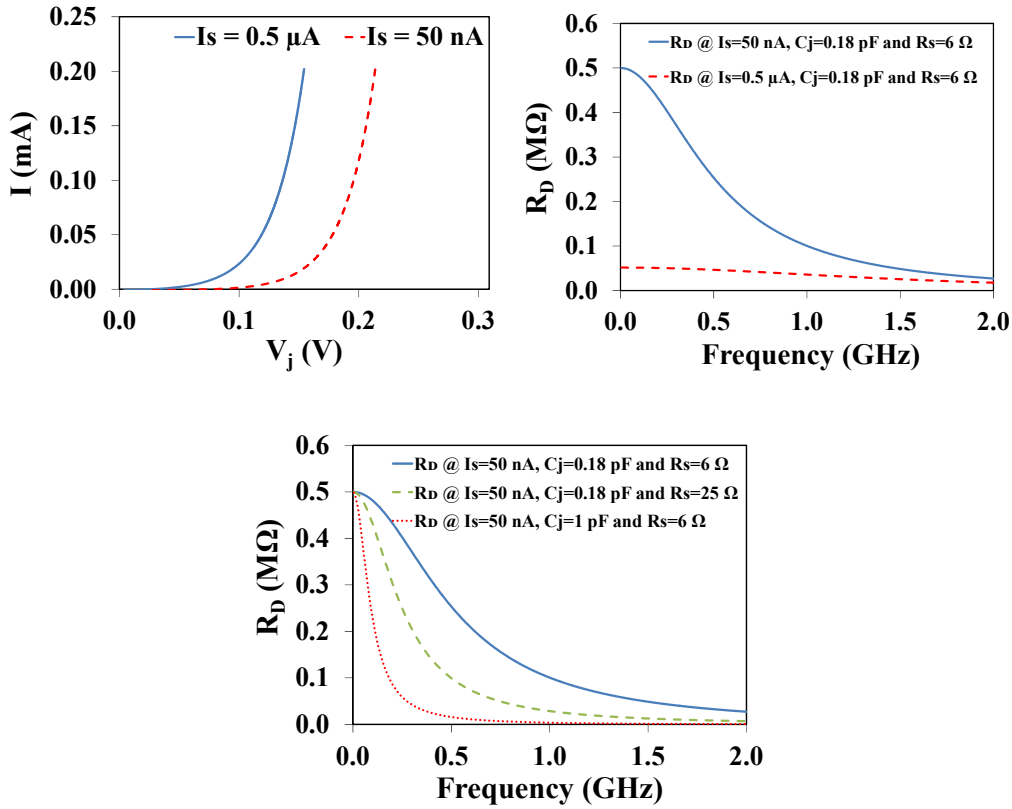

Figure 3. The effect of the changes in the equivalent circuit parameters of a Schottky diode on the parallel resistive impedance, R_D. (Top-left) Effect of the saturation current I_S on the V_j at 25 °C for different currents I passing through the rectifying junction. (Top-right) Schottky diode parallel resistive impedance R_D as a function of different I_S. (Bottom) Schottky diode parallel resistive impedance R_D as a function of different bulk resistances R_S, and junction capacitances C_j.

Figure 3(Top-right) and Figure 3(Bottom) show the calculated effect of I_S, R_S and C_j on the parallel resistive impedance R_D of a diode. From Figure 3(Top-right), as the I_S is increased from 50 nA to 0.5 µA, the R_D reduces. From Figure 3(Bottom), as the junction capacitance C_j is increased from 0.18 pF to 1 pF, the R_D of the diode reduces. By increasing R_S from 6 Ω to 25 Ω, the R_D reduces as well. The results shows that a Schottky diode with a low I_S, R_S and C_j will have high R_D. The results also show that at ultra-high frequency (UHF), the R_D of a diode is in the range of a few kilo-ohms.

2.3. RF power harvesting circuits

Figure 4 shows a fabricated RF harvester realized at 930 MHz on an FR4 printed circuit board using off-the-shelf discrete components. V_S is the input RF voltage. R_A is the RF source resistance. R_L is the DC load resistor. The impedance transformation network is realized with an inductive coil

resonator and a chip capacitor. The unloaded quality factor Q_u of an impedance transformation element is used as the performance parameter for selection a component. Q_u is given by Equation (7), where X_{Coil} and R_{Coil} are the net series reactive and resistive impedance of the inductive transformation element respectively. As can be seen in Figure 3, the R_D of a Schottky diode at about 900 MHz is in the range of a few kilo-ohms. The voltage transformation that can be achieved at the input of a Schottky diode is directly proportional to the $\sqrt{R_D}$ at resonance [5] as in (8). Where V_D is the voltage at the input of the diode rectifier. When the RF voltage amplification at the input of the diode is limited due to a lower value of R_D, the rectifier efficiency is skewed toward diodes with saturation current I_S in the micro-amp range (see Figure 3(Top-left)), since more current I passes through the rectifying junction. Hence the Avago Techologies HSMS-285 series of diodes with I_S = 3 μA were used at 930 MHz to realize the RF harvester.

$$Q_u = \frac{X_{Coil}}{R_{Coil}} \tag{7}$$

$$\frac{V_D}{V_S} \propto \sqrt{\frac{R_D}{R_A}} \tag{8}$$

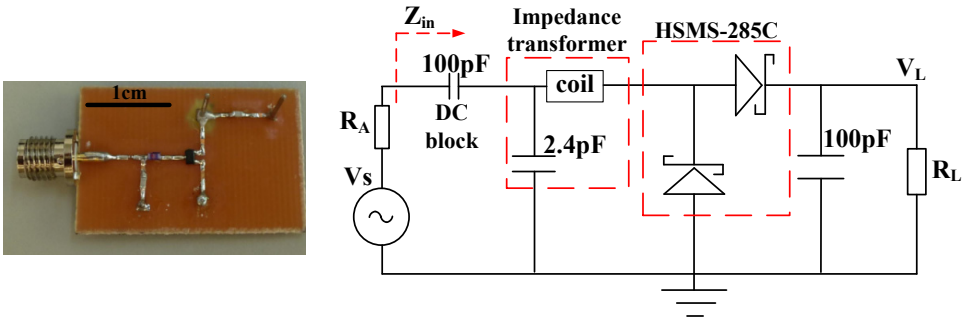

Figure 4. PCB of the realized RF harvester at 930 MHz using a HSMS-285C diode voltage doubler. The HSMS-285C has the following spice parameters I_S = 3 μA, C_j = 0.18 pF and R_S = 25. *Coil* = 38.5 nH at 900 MHz with a Q_u of 69. The chip capacitors have Q_u of about 1000 at 900 MHz.

2.4. Linearized analysis of the RF harvester

The linearized impedance diagram of the RF rectifier shown in Figure 4 is presented in Figure 5. I_{DC} is the same for each diode since two identical diodes are assumed. I_{DC} may be found from (10). P_{in} is the power absorbed at Z_{in} plane as in (9). Where Γ is the reflection coefficient at the Z_{in} plane (see Figure 4). N is the number of doubler stages.

$$P_{in} = P_A\left(1 - |\Gamma|^2\right) \tag{9}$$

$$I_{DC} = \frac{P_{in}}{NV_D} \tag{10}$$

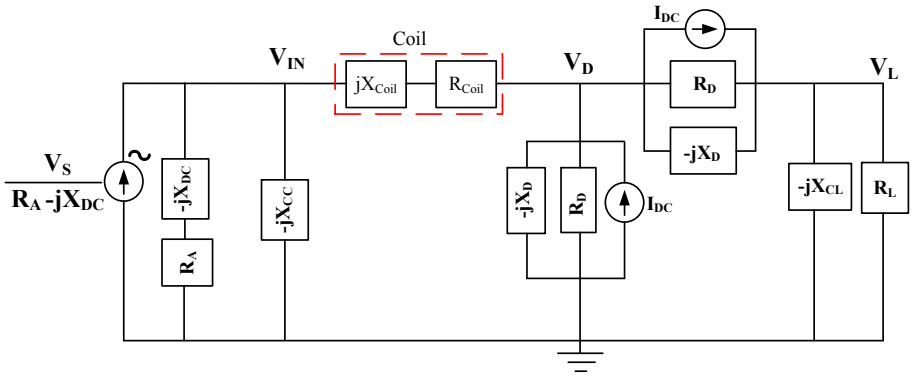

Figure 5. Linearized model of the RF power harvester at 930 MHz. X_{DC} is the reactance of DC block capacitor. X_{CC} is the reactance of 2.4 pF capacitor. R_{Coil} and X_{Coil} are the series resistive and reactive impedance of the coil respectively. X_{CL} is the reactance of the 100 pF capacitor. R_L is the load resistor.

After the linearized model is setup as in Figure 5, the steady state output voltage V_L is found using nodal analysis. From Figure 5, (11), (12) and (13) may be used to determine the voltages at node V_{IN}, V_D and V_L.

$$\frac{V_S}{R_A - jX_{DC}} = V_{IN}\left[\frac{1}{R_A - jX_{DC}} + \frac{1}{-jX_{CC}} + \frac{1}{R_{Coil} + jX_{Coil}}\right] - V_D\left[\frac{1}{R_{Coil} + jX_{Coil}}\right] \tag{11}$$

$$0 = -V_{IN}\left[\frac{1}{R_{Coil} + jX_{Coil}}\right] + V_D\left[\frac{1}{R_{Coil} + jX_{Coil}} + \frac{2}{-jX_D} + \frac{2}{R_D}\right] - V_L\left[\frac{1}{-jX_D} + \frac{1}{R_D}\right] \tag{12}$$

$$I_{DC} = -V_D\left[\frac{1}{R_D} + \frac{1}{-jX_D}\right] + V_L\left[\frac{1}{-jX_{CL}} + \frac{1}{-jX_D} + \frac{1}{R_D} + \frac{1}{R_L}\right] \tag{13}$$

From (11) to (13), the minima of V_L occurs when I_{DC} in the doubler diodes limits to zero. $I_{DC} \approx 0$ implies the diodes are not rectifying at the input RF power level. Hence the output voltage V_L approaches (14). The alternating current (AC) output voltage when $I_{DC} = 0$ is given by V_{L_AC}.

$$V_L \to V_{L\_AC} \tag{14}$$

The maxima of the output voltage V_L approaches (15). For N number of doublers, the upper limit of the V_L is increased by a factor N.

$$V_L \to 2NV_D \tag{15}$$

2.5. Linearized analysis applied to multipliers and multiple input matching circuits

The RF harvester presented for dual-band applications is realized with a coupled matching to provide the multiple resonant frequencies. The presented dual-band harvester which can harvest from

GSM-900 or LTE-800 and GSM-2160 is shown in Figure 6 using a modified voltage quadrupler. The capacitors at the input of the diode chain are connected in parallel, however the capacitors are connected in series at the output of the diode chain. To achieve the additional bands of frequency operation, each input branch into a diode voltage doubler is tuned to a specific frequency; ω_1 (at 935 MHz) and ω_1 (at 2.2 GHz). The resonant frequencies can be approximated by (16). The employed diodes are the HSMS-285C Schottky diodes.

$$\omega_1 \approx \frac{1}{\sqrt{C_{C1}Coil_1}} \text{ and } \omega_2 \approx \frac{1}{\sqrt{C_{C2}Coil_2}} \tag{16}$$

By replacing the diodes in Figure 6 with its linearized model (see Figure 5), its output DC characteristics can be analyzed with the same approach presented in Section 2.4.

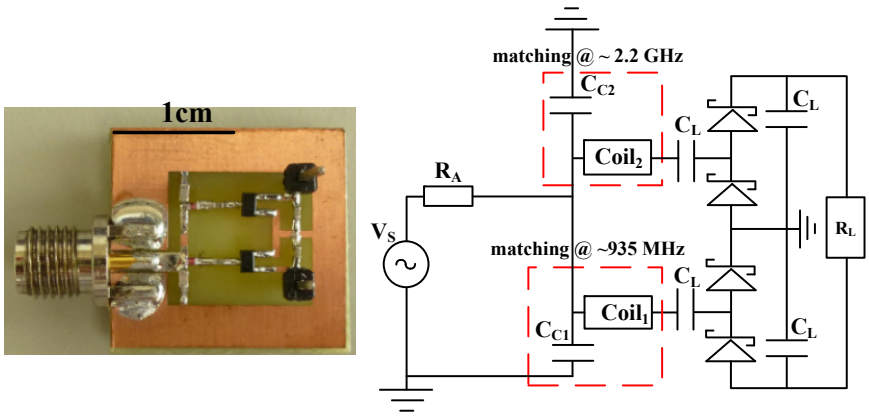

Figure 6. Picture and circuit layout of the dual-band RF harvester. The harvester is matched at 935 MHz and 2.2 GHz. Schottky diodes are HSMS-285x series. C_{C1} = 2.7 pF, $Coil_1$ = 39 nH; $Coil_1$ Q_U @ 900 MHz = 88, C_{C2} =0.8 pF, $Coil_2$ = 2.14 nH; $Coil_2$ Q_U @ 1.7 GHz = 35, C_L =100 pF.

3. Results of RF to DC power transmission

The presented linearized model, ADS HB simulations and measured voltage sensitivity for the harvesters presented in Figure 4 and Figure 6 are shown in Figure 7. For the harvester presented in Figure 4, a DC voltage of 0.4 V across R_L of 0.5 MΩ is measured at −20 dBm input RF power. At −14 dBm input RF power, the harvester as shown in Figure 4 delivers a measured DC voltage of 1 V across a 0.5 MΩ R_L. The harvester achieves a peak efficiency of 24% and 41% at −20 dBm and −10 dBm input RF power respectively for about 6 kΩ R_L when operating at 930 MHz.

For the harvester shown in Figure 6, a DC voltage of 0.43 V across a 0.5 MΩ R_L is measured at −20 dBm input RF power at 935 MHz. At −14.4 dBm input RF power, the harvester as shown in Figure 6 delivers a measured DC voltage of 1 V across a 0.5 MΩ R_L. At 5 dBm input RF power, a DC voltage of 6 V is measured across a 0.5 MΩ R_L at 935 MHz. The harvester achieves a peak efficiency of 16% and 35% at −20 dBm and −10 dBm input RF power respectively for about 10 kΩ R_L when operating at 935 MHz. At 2.2 GHz, an output DC voltage of 0.4 V is measured across a 0.5 MΩ R_L at −10 dBm input RF power. At 2.2 GHz, a peak efficiency of 4% is measured at

−10 dBm input RF power for about 10 kΩ R_L.

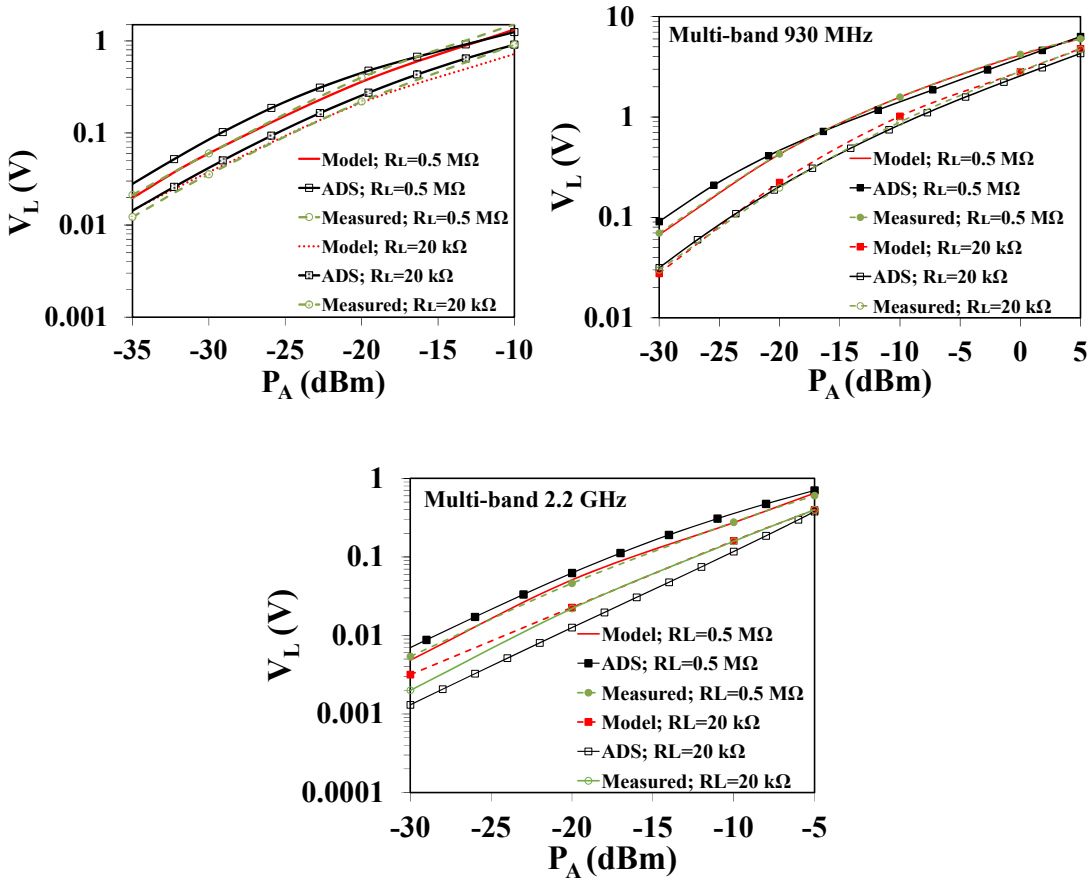

Figure 7. Presented linearized model as compared to Agilent ADS HB simulations and measurements. V_L is the output DC voltage and P_A is the input RF power. (Top-left) Results of the RF harvester as shown in Figure 4. (Top-right) Results of the dual-band RF harvester as shown in Figure 6 at 930 MHz. (Bottom) Results of the dual-band RF harvester as shown in Figure 6 at ~2.2 GHz.

From the results shown in Figure 7, the maximum calculated deviation between measurements and the presented linearized model is 15%. The 15% maximum difference is as a result of calculating the diode R_D and I_{DC}. I_{DC} is dependent on P_A, Γ at Z_{in}, R_D and R_L, as a result any variation such as component tolerances in these parameters affects the estimation of the output DC voltage. R_D is also a function of the R_L and P_A.

4. Circuit Design Considerations

4.1. Circuit performance parameters

The maximum DC load power from the rectifier may be approximated by (17). Where P_{Lmax} is the maximum power delivered to the R_L. The DC load resistance that results in the maximum

efficiency from the RF harvester is given by (18). R_{Lmax} is the DC load resistance R_L that results in the maximum η. For Figure 4, R_{Lmax} is ~6 kΩ. For Figure 6, R_{Lmax} is ~10 kΩ. From (8) and (17), the diode R_D and peak voltage into a diode rectifier V_D, must be high as possible for high voltage sensitivity of the RF harvester.

$$P_{L\,max} \approx \frac{(2NV_D)^2}{2R_L} \tag{17}$$

$$R_{L\,max} \approx 2NR_D \tag{18}$$

From the linearized transfer functions that describe the performance of an RF harvester, a maxima of P_L (P_{Lmax}), R_L (R_{Lmax}), η and γ may be found for any RF harvester topology.

4.2. Rectifying diode selection

The harvester shown in Figure 6 is realized to cover the LTE-800 MHz or GSM 900 MHz and GSM 2110 MHz frequency bands (see Figure 8). Hence the realized harvester loaded quality factor ($\propto \sqrt{R_D/R_A}$) is low at 935 MHz and 2100 MHz.

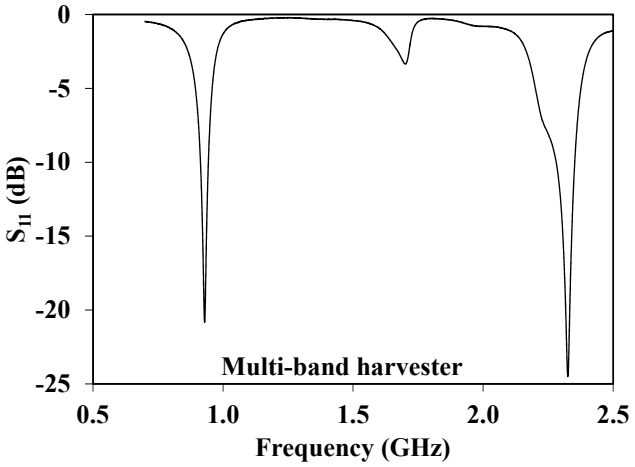

Figure 8. Measured open circuit S_{11} of the dual-band RF harvester. The input RF power level is −15 dBm. The 3-dB return loss frequency bandwidth is 120 MHz around 930 MHz and 200 MHz around 2.2 GHz.

For RF harvesting applications which require such broad-band operations, diodes with low R_D should be considered. Diodes with lower C_j and R_S are always preferable in RF energy harvesting applications. R_S consumes ohmic power, hence the lower the better. C_j in the range of 1 pF reduces the diodes R_D as well as its switching speed. The action of C_j dominates at sufficiently higher diode operating frequencies resulting in lower attainable R_D. Since diodes are more sensitive to high voltage at input power levels less than −10 dBm, a low R_D results in limited voltage transformation. As a result more current goes through the diode and the diodes voltage losses V_j tend to be maximum.

Hence at low diode input R_D, the efficiency of rectifying RF signals is skewed towards the diodes with I_S in the micro-amp range (such as HSMS-285x series), since they have lower peak V_j.

Impedance transformation components with high unloaded quality factor Q_u are always preferable in RF energy harvesting applications. The question always arise whether to use discrete components or transmission lines on a PCB. The unloaded quality factor of a transmission line may be described by (19) [15]. Where F_0 is the transmission line frequency in mega-hetz, A_0 is the attenuation in dB/100 feet at F_0 and VF is the velocity factor.

$$Q_u = \frac{2.7743\, F_0}{A_0\, VF} \tag{19}$$

As an example, an inductive or capacitive transmission line on an FR4 PCB has VF of 0.48 and A_0 of 132 dB/100 feet at 1 GHz. Using (19) and the values of an FR4 transmission line at 1 GHz gives a Q_u of 44. Hence up to 1 GHz, discrete components may be preferred to transmission lines for impedance transformation since chip inductors and capacitors can provide Q_u of up to 80 and 1000 at 1 GHz respectively. However, since inductive transmission lines quality factor is directly proportional to the operating frequency, it may be preferred to discrete inductors at frequencies above 3 GHz.

For RF harvesting applications with input power levels greater than −10 dBm, diodes may be cascaded as in multipliers. This is due to the possible constant output voltage or power of a single rectifier stage after a certain threshold input RF power. The appropriate number of diode doubler stages that strikes a good balance between the losses V_j across the diodes in the multiplier and the power saturation of the rectifier stage must be made. Equation (20) may be used as a guide in choosing the number of rectifier voltage doubler stages N and the peak voltage or power handling capabilities of the rectifier.

$$RF\ \ power \begin{Bmatrix} V_D << V_j; N = 1 \\ V_j << V_D < V_{BV}; N \\ V_D \approx V_{BV}; N + 1 \end{Bmatrix} \tag{20}$$

The maximum DC voltage that can be outputted by a diode is determined by the reverse breakdown voltage V_{BV}. The maximum output DC voltage V_L of a single diode rectifier is $\sim V_{BV}/2$ [2]. Hence the maximum output DC voltage of a diode voltage doubler is $\sim V_{BV}$ and for a multiplier, it is $\sim NV_{BV}$.

5. Wireless RF energy harvesting

5.1. Wireless RF energy transfer in the ISM band 868 MHz.

At 868 MHz, the commercially available Huber+Suhner SPA 860 (1308.17.0058) planar antenna [16] was used as a transmitter. The Huber+Suhner SPA 860 has a gain G_{it} of 8 dBi at 868 MHz and measures 20 cm × 20 cm in size. The antenna presented by Homg-Dean Chen et al. [17] was used to receive the wireless signals at 868 MHz. The antenna by Homg-Dean Chen et al. (see Figure 11) is a dual-band antenna with a 10-dB return loss bandwidth of 90 MHz around 900 MHz and 218 MHz around 1800 MHz. It has a gain G_{ir} of 1 dBi at around 900 MHz and 3 dBi

around 1800 MHz.

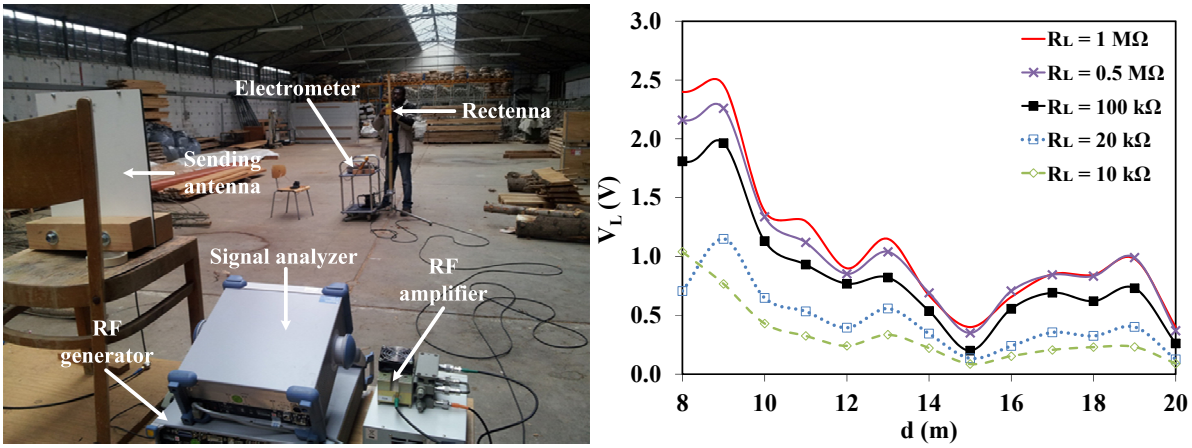

Figure 9. (Left) Picture of the experimental setup for the wireless range measurements at 868 MHz. (Right) Rectenna (antenna + rectifier) receiving range performance by sending P_t of 1 W at 868 MHz. Transmitting antenna size is 20 cm × 20 cm with G_{it} of 8 dBi. Receiving rectenna size is 6 cm × 8 cm. d is the distance between transmitter and rectenna.

The size of the antenna is 6 cm × 8 cm, $\lambda/4$ at 868 MHz. The dual-band rectifier as presented in Figure 6 is used with the antenna for harvesting at 868 MHz. The transmitted RF power P_t was 1 W at 868 MHz. The experimental setup and the wireless range measurements were performed in a warehouse as can be seen in Figure 9 (Left). The sending and the receiving antennas were arranged ~1.5 m above the ground. The rectenna delivered DC voltage was measured with the Keithley 6514 electrometer.

Figure 9(Right) shows the range measurements at 868 MHz. A harvested DC voltage of 0.4 V is measured across a 0.5 MΩ R_L at the distance of 20 m. At 13 m, 1 V DC voltage is measured across a 0.5 MΩ R_L. The far-field results at 868 MHz show that the received power generally degrades with $1/d^2$ as in the Friis equation (21) [18]. Where P_r and P_t are the transmitted and received power respectively. λ is the wavelength of the RF signal. ξ as in (21) is an *additional* parameter in the Friis equation which account for reflections and multi-path propagations of the wireless signals. It can be seen from Figure 9 (Right) that the measured output DC power is modulated by the constructive and destructive interferences along $1/d^2$, since there are farther distances where the delivered power is greater than a nearer range. This is evident at a distance d of 15 m, where a DC output voltage of 0.5 V is harvested as compared to 1 V harvested at d of 19 m for 0.5 MΩ R_L. At 15 m there is destructive interference from to the reflected signals to the direct signals, hence the harvested power is lower than that predicted by the original Friis formula, however, at 19 m, there is constructive interference and the harvested power is higher than that predicted by the original Friis formula.

$$P_r = \xi P_t G_{ir} G_{it} \left(\frac{\lambda}{4\pi d} \right)^2 \tag{21}$$

5.2. Harvesting from ubiquitous GSM signals

To investigate the possible use of ambient RF power sources for operation of remote micro-watt sensors. The RF power levels harvested by a ~λ/4 receiving antenna at 930 MHz was first measured at a distance of about 110 m from a GSM base station. The receiving antenna that was used for this experiment is the dual-band antenna by Homg-Dean Chen et al. [17].

Due to reflections, multi-path propagation and the fact that the transmitting antennas from the GSM base station point at different directions (see Figure 11), the power delivered by the dual-band receiving antenna was not estimated by the Friis formula [18] as in Equation 21. The power delivered by the receiving antenna were made by on-site measurements using a Rohde & Schwarz PR100 RF monitor. From the balcony of a building, about a distance of 110 m from a GSM transceiver base station, the antenna was positioned to harvest the ambient RF power. Figure 10 shows the average (over 5 minutes) harvested RF power levels of the dual-band receiving antenna at a distance of about 110 m from the GSM base station.

The GSM base station is located in the city of Freiburg, Germany at 48.0087,7.829022 coordinates. Table 2 shows the transmitting parameters of the GSM base station.

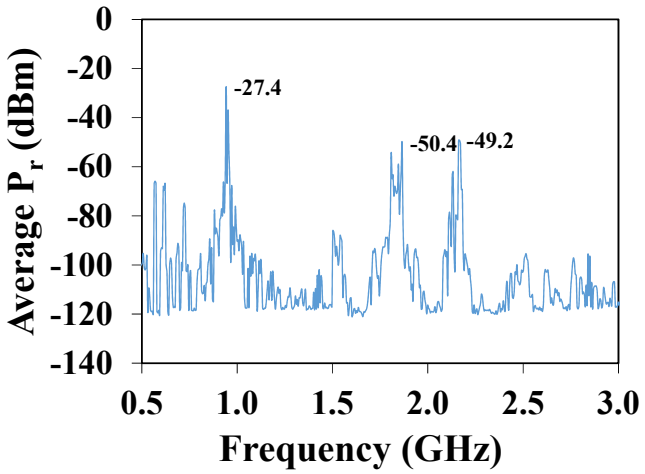

Figure 10. Average (over 5 minutes) ambient RF power delivered by the dual-band antenna at a distance of about 110 m from a GSM base station. Receiving antenna size is 6 cm × 8 cm (~λ/4 at 930 MHz) with a gain of 1 dBi at 930 MHz and 3 dBi at 1800 MHz.

Table 2. Operating parameters of a GSM base station in Freiburg, Germany.

Transmitter	1	2	3	4	5	6
Frequency (MHz)	935	935	2160	2160	2160	811
Transmitting power (W)	102	102	32	32	32	30
Number of channels	1	1	2	2	2	2
Antenna gain (dBi)	15.7	15.7	18.0	18.0	18.0	15.8

Figure 10 shows that the harvested power levels by the dual-band receiving antenna, from the various frequency bands of a GSM base station ranges from −27 dBm to −50 dBm at a distance of about 110 m. Figure 11 shows the output DC voltage from the dual-band rectifier and the dual-band [17] receiving antenna. Figure 11 shows a harvested output DC voltage of about 2.3 V across a ~0.5 MΩ resistor is achieved from the several GSM power sources at a distance of 110 m.

Figure 11. Setup for measuring the power delivered by the GSM base station across a resistive load. The RF to DC rectifier is the circuit as presented in Figure 6 and the antenna is from Homg-Dean Chen et al. [17]. R_L is ~0.5 MΩ. V_L is about 2.3 V.

The delivered DC power by the rectenna is the sum of all the harvested RF signals in the multiple transmitting frequencies (811 MHz, 935 MHz and 2160 MHz) of the base station. The harvested DC power can be approximate by (22) [8]. Where C_1 up to C_N are the transmitting channels. For GSM signals, a channel covers 200 kHz. f_1 and f_2 are the lower and upper band of the RF frequency respectively. f is the frequency. Using this approach, ambient RF power sources in the range of −27 dBm to −50 dBm and from different frequencies can be utilized to power sensors requiring ~1.3 V DC across a 0.5 MΩ and still maintain a ~λ/4 rectenna size.

$$P_{DC} \propto \sum_{C_1}^{C_N} \int_{f_1}^{f_2} P_t \delta f \tag{22}$$

The RF harvester was also loaded with a commercially available TFA 30.5014.02 Thermo-Hygrometer. The Thermo-Hygrometer is normally powered by an LR44 battery requiring 1.3 V to 1.5 V at 3 μA for its continuous operation. It can be seen that the RF harvester was also able to power the sensor through startup-mode and steady state operations (see Figure 12). Since the Thermo-Hygrometer has an input resistance of ~0.5 MΩ and consumes ~1.3 V, the theoretical distance at which the Thermo-Hygrometer may still be powered by the presented RF harvester is about 220 m using the GSM base station.

Figure 12. Using ambient RF GSM power to operate Thermo-Hygrometer sensor. The RF to DC rectifier is as presented in Figure 6.

6. Conclusions

By using a linearized model of a rectifier, a complete description of an RF harvester can be made without compromise. This analysis is confirmed by measured results and HB computer aided simulations for different RF harvester circuit topologies. It is shown that an RF harvester can be optimized using the equations from a linearized RF harvester model. This provides a unique advantage over computer aided simulations which gives little insight into the design trade-off and the effect of the component parameters on the performance of the harvester. The theory presented in this paper could be used for broad design considerations before a specific RF harvester circuit topology is adapted. The theory has been proved by using low cost off-the-shelf components. However the model is equally applicable to custom made designs based on complementary metal-oxide-semiconductor (CMOS) process. It has been shown that using a dual-band RF harvester, ambient RF power sources in the range of −27 dBm to −50 dBm from different frequency bands can be used to provide perpetual energy for operation of wireless remote sensors requiring 1.3 V at 0.5 MΩ. This has been achieved by using rectenna size of ~λ/4 at 930 MHz. In the ISM 868 MHz frequency band, an operation range of 19 m is demonstrated for DC loads requiring 1 V at 0.5 MΩ from a single transmitted signal at indoor conditions.

Acknowledgments

This work is part of the graduate program GRK 1322 Micro Energy Harvesting at IMTEK, University of Freiburg, funded by the German Research Foundation (DFG).

Conflict of Interest

There is no conflict of interest.

References

1. Harrison RG, Le Polozec X (1994) Nonsquarelaw behavior of diode detectors analyzed by the Ritz-Galerkin method. *Microw Theory Tech IEEE Trans* 42: 840–846.
2. McSpadden JO, Fan I, Chang K (1998) Design and experiments of a high-conversion-efficiency 5.8-GHz rectenna. *Microw Theory Tech IEEE Trans* 46: 2053–2060.
3. Curty J-P, Joehl N, Krummenacher F, et al. (2005) A model for μ-power rectifier analysis and design. *Circuits Syst Regul Pap IEEE Trans* 52: 2771–2779.
4. Barnett RE, Liu J, Lazar S (2009) A RF to DC voltage conversion model for multi-stage rectifiers in UHF RFID transponders. *Solid-State Circuits IEEE* 44: 354–370.
5. Nimo A, Grgić D, Reindl LM (2012) Optimization of passive low power wireless electromagnetic energy harvesters. *Sensors* 12: 13636–13663.
6. Nimo A, Grgić D, Reindl LM (2012) Ambient electromagnetic wireless energy harvesting using multiband planar antenna. *Systems Signals Devices (SSD), 9th International Multi-Conference on* 1–6.
7. Sample A, Smith JR (2009) Experimental results with two wireless power transfer systems. *Proceedings of the 4th international conference on Radio and wireless symposium*, San Diego, CA, USA, 16–18.
8. Mikeka C, Arai H (2011) Design issues in radio frequency energy harvesting system. *Sust Energ Harvesting Technologies—Past Present and Future*, InTech.
9. Vyas RJ, Cook BB, Kawahara Y, et al. (2013) E-WEHP: A batteryless embedded sensor-platform wirelessly powered from ambient digital-TV signals. *Microw Theory Tech IEEE Trans* 61: 2491–2505.
10. Pinuela M, Mitcheson PD, Lucyszyn S (2013) Ambient RF energy harvesting in urban and semi-urban environments. *Microw Theory Tech IEEE Trans* 61: 2715–2726.
11. Joe J, Chia M, Marath A, et al. (1997) Zero bias schottky diode model for low power, moderate current rectenna. *DETS'97 Proc*.
12. Watson HA (1969) Schottky-barrier Devices. *Microwave semiconductor devices and their circuit applications*, New York; Maidenhead: McGraw-Hill.
13. Maas SA (2003) Harmonic-Balance Analysis and Related Methods. *Nonlinear microw RF circuits*, Boston, MA: Artech House.
14. Sah C-T (1991) P/N and Other Junction Diodes. *Fundamentals of solid-state electronics*, Singapore; River Edge, NJ: World Scientific.
15. Audet J (2006) Q Calculations of L-C Circuits and Transmission Lines: A Unified Approach. *QEX Mag* 43–51.
16. HUBER+SUHNER (2010) Rfid reader antenna: Spa 860/65/9/0/v (1308.17.0005).
17. Chen H, Chen W, Cheng Y, et al. (2003) Dualband meander monopole antenna. *Antennas Propagation Society Int Symp IEEE* 3: 48–51.
18. Friis HT (1946) A Note on a Simple Transmission Formula. *Proc IRE* 34: 254– 256.